PROCEEDINGS A

rspa.royalsocietypublishing.org

Research

Cite this article: Lai C-Y, Zheng Z, Dressaire E, Wexler JS, Stone HA. 2015 Experimental study on penny-shaped fluid-driven cracks in an elastic matrix. *Proc. R. Soc. A* **471**: 20150255. http://dx.doi.org/10.1098/rspa.2015.0255

Received: 17 April 2015
Accepted: 18 September 2015

Subject Areas:
fluid mechanics, geophysics

Keywords:
thin films, fluid–structure interactions, geophysical and geological flows

Author for correspondence:
Howard A. Stone
e-mail: hastone@princeton.edu

Electronic supplementary material is available at http://dx.doi.org/10.1098/rspa.2015.0255 or via http://rspa.royalsocietypublishing.org.

THE ROYAL SOCIETY PUBLISHING

Experimental study on penny-shaped fluid-driven cracks in an elastic matrix

Ching-Yao Lai[1], Zhong Zheng[1], Emilie Dressaire[2], Jason S. Wexler[1] and Howard A. Stone[1]

[1]Department of Mechanical and Aerospace Engineering, Princeton University, Princeton, NJ 08544, USA
[2]Department of Mechanical and Aerospace Engineering, New York University Polytechnic School of Engineering, Brooklyn, NY 11201, USA

When a pressurized fluid is injected into an elastic matrix, the fluid generates a fracture that grows along a plane and forms a fluid-filled disc-like shape. We report a laboratory study of such a fluid-driven crack in a gelatin matrix, study the crack shape as a function of time and investigate the influence of different experimental parameters such as the injection flow rate, Young's modulus of the matrix and fluid viscosity. We choose parameters so that effects of material toughness are small. We find that the crack radius $R(t)$ increases with time t according to t^{α} with $\alpha = 0.48 \pm 0.04$. The rescaled experimental data at long times for different parameters collapse based on scaling arguments, available in the literature, showing $R(t) \propto t^{4/9}$ from a balance of viscous stresses from flow along the crack and elastic stresses in the surrounding matrix. Also, we measure the time evolution of the crack shape, which has not been studied before. The rescaled crack shapes collapse at longer times and show good agreement with the scaling arguments. The gelatin system provides a useful laboratory model for further studies of fluid-driven cracks, which has important applications such as hydraulic fracturing.

1. Introduction

Fluid-driven cracks in an elastic material are encountered when studying many problems in geophysics such as magma transport, which is relevant to crustal processes, and hydraulic fracturing, which is used as part of a method to extract oil and gas from an underground reservoir. In the magma transport problems, the main

driving force for crack propagation is buoyancy from the density difference between the fluid-filled crack (magma) and the ambient elastic material (rock) [1–4]. In contrast, in the process of hydraulic fracturing, the propagation of a crack in a solid matrix is driven by the invasion of pressurized water or other fluids into rock. In this paper, we report an experimental study inspired by hydraulic fracturing.

The process of hydraulic fracturing has been modelled using a combination of linear elastic theory and fluid mechanics. The shape of the crack opened by normal stresses in an elastic medium is modelled conventionally as a disc- or penny-shaped crack [5,6]. Khristianovic & Zheltov [7] connected the crack problem with fluid flow to model hydraulic fracturing and subsequently the fluid-driven penny crack problem has been studied extensively [2,8–10]. Spence & Sharp [11] developed a theory for fluid-driven cracks in an infinite elastic medium, assuming zero energy dissipation via crack tip extension (zero toughness). Also, Detournay and co-workers [8,12] focused on the dynamics of the crack tip region and showed that the ratio between energy dissipation via crack tip extension and viscous dissipation accompanying fluid flow significantly affects the crack propagation behaviour [9,10].

One of the classical experimental works on hydraulic fracturing was reported by Hubbert & Willis [13], who investigated the elastic field around the injection point, and its effect on the crack orientation. In particular, these authors conducted cracking experiments in gelatin and focused on the early formation of the crack. Also, Bunger [14] developed a method to measure the thickness of a fluid-driven crack propagating between cemented polymethyl methacrylate (a type of plastic) blocks and validated the behaviours at the crack tip region [10], when the dominant mechanism of energy dissipation comes from either viscous flow [2,11] or crack tip extension [6]. Other gelatin experiments on fluid-driven crack propagation were inspired by magma propagation problems, where buoyancy is the driving force [3,4,15]. To date, there has been little experimental attention given to the time dependence of the crack growth and shape.

In this report, we study the dynamics of fluid-driven cracks using laboratory experiments in gelatin. While there are many experiments using gelatin, which focused on buoyancy-driven cracks [3,4,15], and some studies on the static shape of penny-shaped cracks where a high fluid pressure is the driving force for crack propagation [14,16], we investigate the time evolution of the shape of fluid-driven cracks. Our experimental observations exhibit good agreement with the predictions of Spence & Sharp [11].

2. Fluid-driven cracks in an elastic matrix

(a) Experimental methods and observations

To study an idealized model for hydraulic fracturing, we injected fluid at a constant flow rate Q into an elastic material and studied the propagation of a single crack generated by the invasion of the fracturing liquid. We chose gelatin as the elastic material since it is commonly used in the geosciences [3,4,13,15,17,18] because it mimics the elastic and brittle properties of rocks. Also, gelatin is transparent, which allows detailed imaging.

We prepared a reservoir of solid gelatin ($150 \times 150 \times 113$ mm), as shown in figure 1. Young's modulus was varied by changing the concentration of the gelatin powder (Gelatin type A; ThermoFisher Scientific, USA) and measured via indentation tests [19], with values ranging from 95 ± 9.5 kPa to 275 ± 27.5 kPa. A syringe filled with the fracturing liquid was connected to a needle with one end placed inside the gelatin. The liquid injection rate was set by the syringe pump (PhD Ultra; Harvard Apparatus). Different types of liquids and their properties are listed in §2c. Two Nikon D5100 cameras (1280×720 pixels, frame rate = 24 fps) were placed on the top and the side to record the three-dimensional shape of the crack, with the camera configuration shown in figure 1.

The typical features of a fluid-driven crack are shown in figure 2. The propagation of the liquid (dyed) can be observed clearly through the transparent gelatin. As the fracturing liquid was

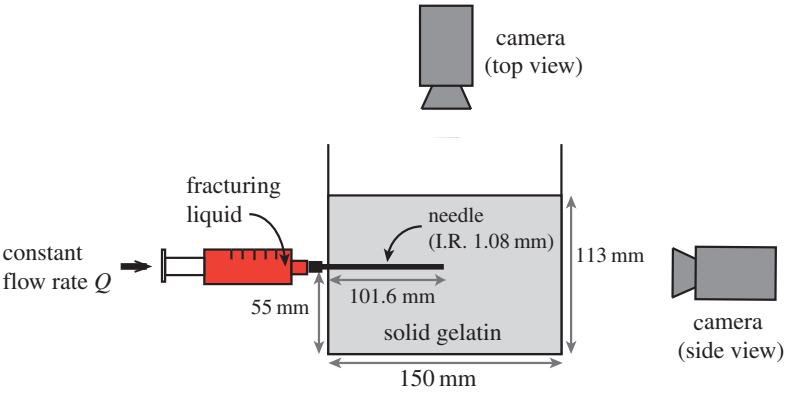

Figure 1. Schematic diagram of the experimental set-up. Fracturing liquid was injected with a constant flow rate Q into an elastic gelatin reservoir. The flow forced fracturing liquid to move forward and eventually fractured the gelatin. I.R. represents inner radius. (Online version in colour.)

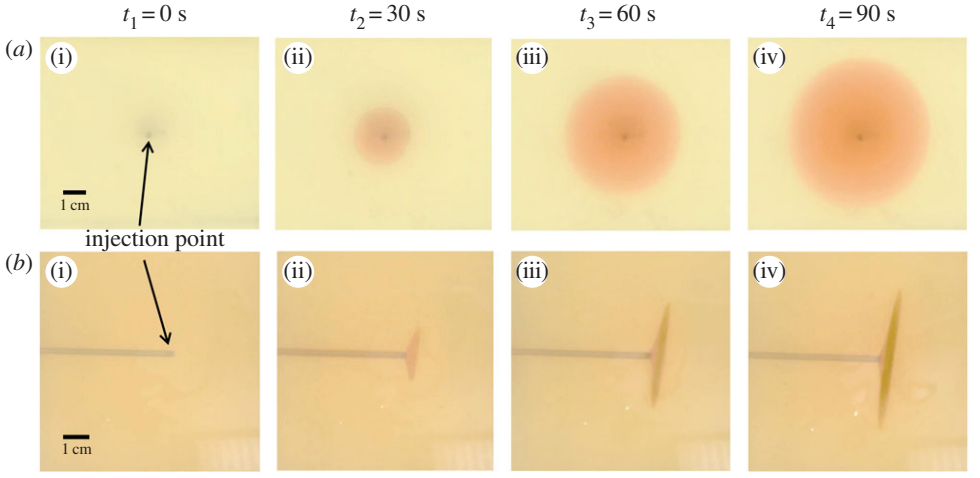

Figure 2. Time evolution of the fluid-driven crack geometry from (*a*) the side view and (*b*) the top view. As the fracturing liquid (silicone oil of viscosity 1020 mPa · s, dyed) was injected into gelatin with a constant flow rate ($Q = 10$ ml min^{-1}), a penny-shaped crack was created and propagated radially along a plane. (Online version in colour.)

injected into the gelatin reservoir, the liquid propagated radially along a disc-like crack. We used silicone oils as the fracturing liquid, which is impermeable with the gelatin. The orientation of the fracture is usually perpendicular to the needle. The disc-like crack is referred to as a penny-shaped crack in the previous theoretical studies [5,9], which will be discussed in the next section.

(b) Summary of scaling arguments for a fluid-driven crack

Theory and scaling arguments for a fluid-driven crack have been presented by Spence & Sharp [11]. They considered the problem of fluid injection from a point source into an unbounded linear elastic medium. A crack is initiated in the elastic medium and the shape of the axisymmetric crack is sketched in figure 3. With a constant injection flow rate Q, the crack of radius $R(t)$ propagates in a plane and elastically deforms in the direction perpendicular to the plane. The two main physical mechanisms considered here are (i) the elastic deformation of a crack and (ii) the laminar flow driven by the radial pressure gradient in a narrow crack, with maximum half-width $W \ll R$, where lubrication theory is applicable.

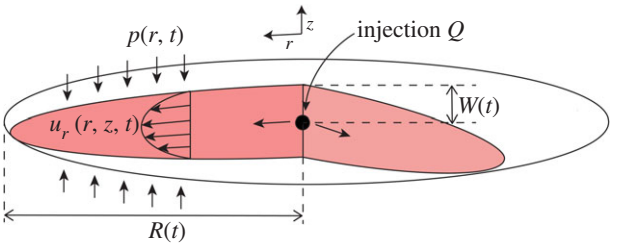

Figure 3. Schematic diagram of a penny-shaped crack. The fluid is injected at a volumetric flow rate Q, the flow along the crack is indicated, and the growing crack radius $R(t)$ and half maximum thickness $W(t)$ are shown. (Online version in colour.)

Table 1. A summary of the scaling arguments for the time dependence of the crack radius, crack thickness and fluid pressure.

property	scaling arguments
crack radius	$R \approx \left(\frac{Q}{4\pi}\right)^{1/3} \left(\frac{E}{6\mu\,(1-\sigma^2)}\right)^{1/9} t^{4/9}$
crack thickness	$W \approx \left(\frac{Q}{4\pi}\right)^{1/3} \left(\frac{E}{6\mu\,(1-\sigma^2)}\right)^{-2/9} t^{1/9}$
fluid pressure	$p \approx \frac{E}{2\,(1-\sigma^2)} \left(\frac{E}{6\mu\,(1-\sigma^2)}\right)^{-1/3} t^{-1/3}$

The order of magnitude of terms in the governing equations for a fluid-driven crack in an elastic matrix of zero toughness [11] (equations (A 1), (A 3) and (A 4) in appendix A) can be written as

$$p \approx \frac{W}{R}\frac{E}{2(1-\sigma^2)}, \quad \frac{W}{t} \approx \frac{1}{3\mu}\frac{W^3 p}{R^2} \quad \text{and} \quad 4\pi WR^2 \approx Qt, \tag{2.1a,b,c}$$

where σ is Poisson's ratio, E is Young's modulus, p is the elastic pressure applied on the crack surface, and $R(t)$ and $W(t)$ are, respectively, the crack radius and half maximum crack thickness. With E, σ, μ and Q as fixed parameters in one experiment and three equations (2.1a,b,c), we seek the approximate time dependence of the three dependent variables (p, W, R). A summary of the scaling arguments is presented in table 1, which will be used to rescale our experimental data in the next section.

(c) Experimental results

We measured the crack radius $R(t)$ as a function of time t for different fracturing liquid viscosities μ, gelatin Young's moduli E and injection flow rates Q. The plot of R versus t is shown in figure 4a. Each individual dataset appears nearly linear on the log–log graph, with approximately the same slope, but offset in position.

We next compare our results with the scaling arguments of §2b, which neglect the influence of matrix toughness. The relative importance of toughness-related stresses Δp_f relative to viscous stresses Δp_v, based on the scaling arguments, is presented in appendix B. For the experiments reported here, $\Delta p_f / \Delta p_v < 1$, as we next show, the data can be explained with the use of viscosity-dominated scaling arguments.

We now rescale the radius based on the scaling law for R as shown in table 1. We observe that the curves collapse at the longer times, as shown in figure 4b. The black line is fitted from

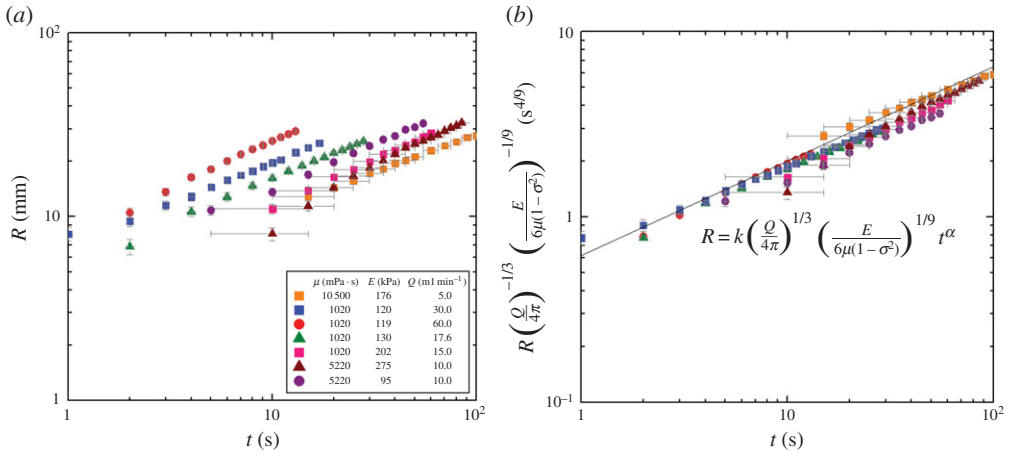

Figure 4. (*a*) Dependence of the crack radius R on time t for different fracturing liquid viscosities μ, gelatin Young's moduli E and injection flow rates Q. The origin for time is chosen to be the moment when the liquid is injected into the gelatin. (*b*) The rescaled crack radius versus time. The dark line with a pre-factor $k = 0.62 \pm 0.14$ and exponent $\alpha = 0.48 \pm 0.04$, obtained from fitting the late dynamics (and averaging over all the datasets shown), agrees with the scaling law expected for $R(t)$ (table 1). Errors have been estimated based on all measurement uncertainties and property values. (Online version in colour.)

Table 2. Silicone oils (Sigma-Aldrich, USA) of different viscosities are used as the fracturing liquids in our experiments. The viscosities were measured using a rheometer (Physica MCR 301).

fluid type	viscosity (at 23°C)
silicone oil 1	10 500 ± 20 mPa · s
silicone oil 2	1020 ± 5 mPa · s
silicone oil 3	5220 ± 5 mPa · s

data points in the late time periods, with an averaged pre-factor $k = 0.62 \pm 0.14$ and exponent $\alpha = 0.48 \pm 0.04$, which agrees with the $\frac{4}{9}$ power law shown in table 1. All of the results show similar quantitative trends at long times. The error bars are estimated according to the measurement uncertainties, such as Young's modulus (±10%), viscosity (typical values given in table 2), crack radius (±0.66 mm) and time (±5 s). Errors in time appear when determining $t = 0$ at which the liquid emerges at the needle tip. A representative value for the effective Reynolds number of fluid flow in the crack can be estimated: when silicone oil ($\rho \approx 980\,\mathrm{kg\,m^{-3}}$, $\mu \approx 1\,\mathrm{Pa \cdot s}$) is injected into a gelatin of Young's modulus $E \approx 119$ kPa at flow rate $Q = 60\,\mathrm{ml\,min^{-1}}$, a penny-shaped crack is generated with half thickness $W \approx 1.18$ mm and radius $R \approx 20.1$ mm at $t \approx 6$ s (half way through the experiment). Then, $Re_{\mathrm{eff}} = \rho U(2W)^2/(\mu R) = \rho QW/(\pi R^2 \mu) \approx 9.1 \times 10^{-4}$.

We observe slight spreading in the rescaled data in figure 4*b*, which is likely to be due to minor effects that were not considered in the model, for example the finite size of the gelatin matrix. Also, the early time dynamics and variability can be other reasons for the small variations illustrated in figure 4.

3. Crack thickness measurements

We have observed penny-shaped fluid-driven cracks in our gelatin experimental system. The simplicity of such a geometry also allows us to conduct experiments to measure the crack shape as a function of time.

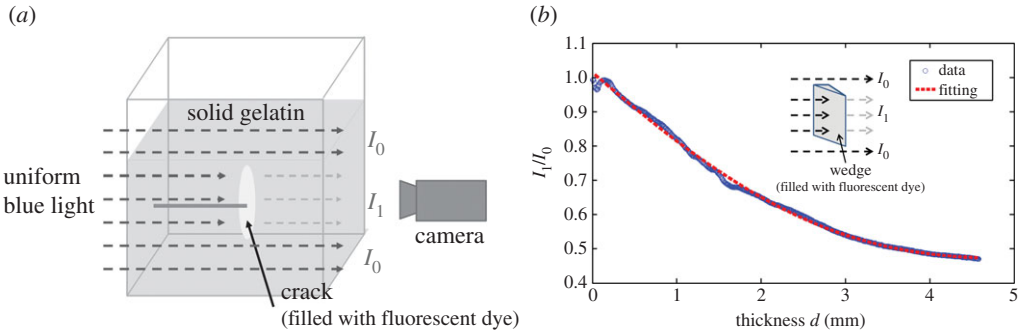

Figure 5. (*a*) An illustration of the method to measure the thickness of the crack. The fracturing liquid was dyed with fluorescein, which absorbs the background uniform blue light (intensity I_0). A camera facing the background light captures the transmitted light (intensity I_1), which is not absorbed by fluorescein. (*b*) Calibration of dyed fluid shown with thickness, d, versus the normalized blue light intensity, I_1/I_0. The circles represent the experimental data and the dashed curve is the fitting curve (equation (C 1)) we used in our data analysis. Note that the experimental data points near $d = 0$ are at the boundary of the wedge and are not reliable. (Online version in colour.)

(a) Methods

We developed an imaging technique to measure the thickness of a crack based on a decrease in the background light intensity as it passes through the dye-filled crack. A similar method has been used in previous studies [14,16].

We used a background blue light source with a uniform light intensity (figure 5*a*). The fracturing liquid is mixed with fluorescent dye (30 µl fluorescent yellow 131 SC + 10 ml tap water), which absorbs blue light and emits light at a longer wavelength. For a specific type of fluid, the amount of absorption is related to the thickness of the fluid through which the light passes. We recorded the intensity distribution of blue light behind the fluid-filled crack I_1 using a Nikon D5100 camera (4928 × 3264 pixels). The thicker the crack, the more blue light is absorbed by fluorescent dye particles, and the weaker the output light intensity captured by the camera. A separate calibration experiment was performed to obtain the relation between the thickness of the liquid, d, and the normalized blue light intensity, I_1/I_0, as shown in figure 5*b*. The crack thickness in a given experiment follows by identifying $d = 2w(r, t)$. A detailed description of the calibration method is provided in appendix C.

(b) Time evolution of crack thickness profile

The crack thickness $2w(r, t)$ is measured as a function of both position and time, as shown in figure 6*a*. The thickness measurements were taken every 3 s. $w(r, t)$ is obtained by dividing the measured crack thickness by a factor of 2, assuming the shape of the crack is symmetric about the z-axis. The $t = 0$ curve, when there is no fluid in the crack, is a horizontal line in figure 6*a*. When fluid injection starts, both the crack radius and thickness increased with time. We note that in a small region at the centre of the crack (of width 7.8 mm) light was blocked due to the needle used for fluid injection. There are data points at each pixel across the crack radius except in this central region (figure 6).

(c) Rescaled crack thickness profiles

According to the scaling arguments for crack radius and thickness, shown in table 1, we rescaled the crack shapes. These measurements thus serve as an additional means for assessing details of the fluid–elastic theory. As shown in figure 6*b*, the rescaled crack thickness profiles collapsed after approximately 12 s for this particular experiment.

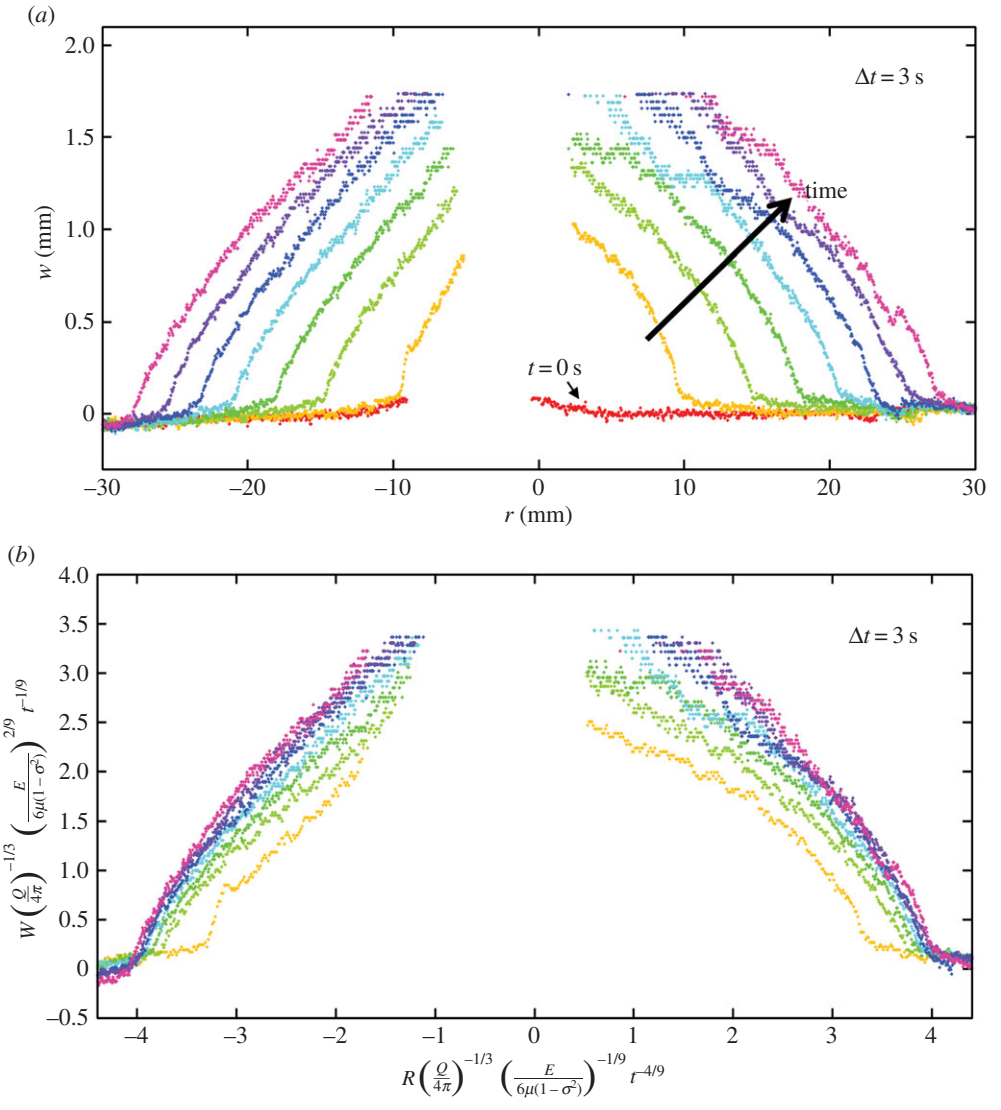

Figure 6. (*a*) Time evolution of the crack thickness profile $w(r, t)$, measured across a fixed cross-section. w is half of the measured crack thickness, assuming the crack is symmetric across the z-axis. The data points of the same darkness represent the measured thickness at each pixel along the r-axis. The time difference between curves is $\Delta t = 3$ s. The time $t = 0$ is defined as the moment when liquid is injected into gelatin. Experimental parameters: $\mu = 1020$ mPa · s, $E = 457$ kPa, $Q = 15$ ml min^{-1}. (*b*) The rescaled crack thickness profile based on the scaling laws (table 1). (Online version in colour.)

4. Concluding remarks

In this paper, we experimentally studied the propagation of a fluid-driven crack in an elastic matrix of negligible toughness. We injected fluid into solid gelatin and recorded the growth of the crack radius and the shape of the crack. We investigated the influence of the injection flow rate Q, fluid viscosity μ and gelatin Young's modulus E. The crack radius R shows a $\frac{4}{9}$ power-law dependence on time, and the experimental data for different parameters (Q, μ, E) collapse based on the viscously dominated scaling arguments of Spence & Sharp [11]. The time evolution of the crack shape is also measured, and the dimensionless crack profiles collapse at late times.

Our experimental system is shown to be robust and provides a useful laboratory model for further studies of fluid-driven cracks, such as poroelastic effects which have been neglected in

our experiment. In addition, the backflow as the elastic matrix relaxes is another area for future research using the experimental system.

Data accessibility. Data in the work are available as the electronic supplementary material.
Authors' contributions. All authors contributed to all aspects of this work.
Competing interests. We declare we have no competing interests.
Funding. This work is partly sponsored by the Princeton University Carbon Mitigation Initiative, the Andlinger Center for Energy and Environment at Princeton University and the National Science Foundation (grant AWD 1004466).
Acknowledgements. We thank Jie Feng, Herbert Huppert, Hyoungsoo Kim, Janine Nunes, Guy Ramon and Allan Rubin for helpful discussions.

Appendix A. Governing equations for fluid-driven cracks in an elastic matrix

This section provides a summary of a model developed by Spence & Sharp [11] for fluid-driven cracks in an elastic medium when material toughness is negligible (figure 3).

(a) Elastic pressure

Across the surface of the crack, the shear traction is assumed to be negligible. The fluid stress applied on the wall of the crack is in the normal direction to the surface, which balances the elastic stress due to deformation. The elastic pressure $p(r,t)$, regarded as the excess pressure above the hydrostatic value, is obtained as a function of the crack shape, which, for an axisymmetric disc-shaped crack of radius $R(t)$ and thickness $2w(r,t)$, is

$$p(r,t) = -\frac{E}{2(1-\sigma^2)} \int_0^{R(t)} M\left(\frac{r}{s}\right) \frac{\partial w(s,t)}{\partial s} \frac{1}{s} \mathrm{d}s, \tag{A 1}$$

where M is a kernel for the elastic response, σ is Poisson's ratio and E is Young's modulus. A detailed derivation and the expression for the kernel function M based on classical linear elasticity theory can be found in Sneddon [20], Spence [21] and Spence & Sharp [11].

(b) Laminar flow in the crack

The lubrication approximation is applicable for fluid flow in a narrow crack. Cylindrical coordinates (r,z) are used with z transverse to the radial direction of crack propagation. The pressure $p(r,t)$ is assumed uniform across the crack width, so that the pressure-driven flow has a velocity profile $u_r(r,z,t)$:

$$u_r(r,z,t) = \frac{1}{2\mu} \frac{\partial p}{\partial r} (z^2 - w^2(r,t)). \tag{A 2}$$

Substituting the vertically averaged velocity into the continuity equation, we obtain the Reynolds equation for the crack width $2w(r,t)$:

$$\frac{\partial w(r,t)}{\partial t} = \frac{1}{3\mu r} \frac{\partial}{\partial r} \left(r w^3(r,t) \frac{\partial p}{\partial r} \right). \tag{A 3}$$

The physical picture embedded in this equation is that the crack is opened up by the pressure from an incompressible fluid flow. In addition, the global conservation of fluid volume gives

$$4\pi \int_0^{R(t)} r w(r,t)\, \mathrm{d}r = Qt, \tag{A 4}$$

for constant fluid injection at flow rate Q. In the main text, §2b, we summarize the scaling arguments based on equations (A 1), (A 3) and (A 4) for the time dependence of the crack radius, crack thickness and fluid pressure, respectively.

Table 3. Coefficients in equation (C 1).

coefficients	C_0	C_1	C_2	C_3	C_4
units	—	mm^{-1}	mm^{-2}	mm^{-3}	mm^{-4}
values	1.014	−0.2084	0.0026	0.0066	0.0006

Appendix B. Toughness-related stress and viscous stress

In this section, we estimate the relative importance of toughness-related stress Δp_f to viscous stress Δp_v. Considering a penny-shaped crack (mode I), the stress intensity factor K_I is related to the elastic pressure $p(r,t)$ via [6,9]

$$K_I = \frac{2}{\sqrt{\pi R}} \int_0^{R(t)} \frac{p(r,t)}{\sqrt{R^2 - r^2}} r \, dr. \tag{B 1}$$

Crack propagation occurs once $K_I = K_{IC}$ [1,2,9], where $K_{IC} = \sqrt{2\gamma_s E}$ is a material property called the fracture toughness [4,15], and γ_s is the surface energy of the elastic matrix. Thus, an estimate of the required elastic pressure for crack propagation is $\Delta p_f \approx K_{IC}/\sqrt{R} \approx \sqrt{\gamma_s E/R}$. In addition, the viscous stress Δp_v can be estimated using Reynolds equation (A 3) and the conservation of fluid volume (A 4): $\Delta p_v \approx \mu Q/W^3$.

Thus, the relative importance of toughness-related stresses to viscous stresses is $\Delta p_f/\Delta p_v \approx \gamma_s^{1/2} E^{1/2} W^3/(R^{1/2}\mu Q)$. After substituting into the scaling laws for W and R presented in table 1, we obtain

$$\frac{\Delta p_f}{\Delta p_v} \approx \frac{(1-\sigma^2)^{13/18} \gamma_s^{1/2} t^{1/9}}{\mu^{5/18} Q^{1/6} E^{2/9}}. \tag{B 2}$$

The ratio represented by equation (B 2) was identified in a previous theoretical study including toughness effects [9].

For gelatin, we use $\sigma = 0.5$ and $\gamma_s \approx 1\,J\,m^{-2}$, which was found experimentally by Menand & Tait [4]. For different experimental parameter sets presented in figure 4, we find that $\Delta p_f/\Delta p_v$ ranges from 0.62 to 0.98 (half way through an experiment). This ratio indicates that the effect of toughness is smaller than the viscous effects, which is consistent with our data collapsing for a wide range of viscosities based on the viscosity-dominated scaling laws.

Appendix C. Calibration method for crack thickness measurements

To find the relationship between the transmitted blue light intensity and the thickness of a fluid-filled crack, a calibration experiment was conducted. We made a wedge with a linearly increasing thickness and filled the wedge with dye-laden fluid (figure 5*b*). Then, we measured the distribution of blue light intensity after light passes through the fluid-filled wedge, which is a function of thickness, d. Note that gelatin particles also absorb light. Thus, when performing the calibration, we have to place the wedge in the middle of the gelatin reservoir to make sure that the absorption from gelatin particles is taken into account. The decrease in blue light intensity due to absorption by gelatin particles can be eliminated via normalizing the blue light intensity, I_1, that passed through the fluid-filled crack by the uniform blue light intensity, I_0, that only travels through gelatin to the camera.

Thus, an empirical curve of the decrease of blue light intensity, I_1/I_0, due to fluorescence absorption versus wedge thickness, d, is obtained, as was shown in figure 5*b*. The experimental data were fitted by a polynomial curve with the coefficients given in table 3,

$$\frac{I_1}{I_0} = C_0 + C_1 d + C_2 d^2 + C_3 d^3 + C_4 d^4. \tag{C 1}$$

Given the calibration curve (equation (C 1)), we can transform the distribution of measured blue light intensity to the thickness of the fluid-filled crack, i.e. $2w = d$. The results of our time-dependent measurements were shown in figure 6*a*. Note that, for a certain fluid thickness d, light travels through gelatin for a slightly different distance between the calibration experiment and the fluid-driven crack experiment. However, since the change in the attenuation of light due to the change in gelatin path length is small compared with the attenuation of light due to the passage through the liquid, the small variation of travel distance in gelatin is negligible.

References

1. Rubin AM. 1995 Propagation of magma-filled cracks. *Annu. Rev. Earth Planet. Sci.* **23**, 287–336. (doi:10.1146/annurev.ea.23.050195.001443)
2. Lister JR, Kerr RC. 1991 Fluid-mechanical models of crack propagation and their application to magma transport in dykes. *J. Geophys. Res.* **96**, 10 049–10 077. (doi:10.1029/91JB00600)
3. Takada A. 1990 Experimental study on propagation of liquid-filled crack in gelatin: shape and velocity in hydrostatic stress condition. *J. Geophys. Res.* **90**, 8471–8481. (doi:10.1029/JB095iB06p08471)
4. Menand T, Tait SR. 2002 The propagation of a buoyant liquid-filled fissure from a source under constant pressure: an experimental approach. *J. Geophys. Res. Solid Earth* **107**, ECV 16-1–ECV 16-14. (doi:10.1029/2001JB000589)
5. Sneddon IN. 1946 The distribution of stress in the neighborhood of a crack in an elastic solid. *Proc. R. Soc. A* **187**, 299–260. (doi:10.1098/rspa.1946.0077)
6. Rice JR. 1968 Mathematical analysis in the mechanics of fracture. In *Fracture: an advanced treatise. Mathematical Fundamental*, vol. 2 (ed. H Liebowitz), pp. 191–311. New York, NY: Academic Press.
7. Khristianovic SA, Zheltov YP. 1955 Formation of vertical fractures by means of highly viscous liquid. *Proc. 4th World Petrol. Congr.* **2**, 576–586.
8. Garagash D, Detournay E. 2000 The tip region of a fluid-driven fracture in an elastic medium. *J. Appl. Mech.* **67**, 183–192. (doi:10.1115/1.321162)
9. Savitski AA, Detournay E. 2002 Propagation of a penny-shaped fluid-driven fracture in an impermeable rock: asymptotic solutions. *Int. J. Solids Struct.* **39**, 6311–6337. (doi:10.1016/S0020-7683(02)00492-4)
10. Garagash D, Detournay E. 2005 Plane-strain propagation of a fluid-driven fracture: small toughness solution. *J. Appl. Mech.* **72**, 916–928. (doi:10.1115/1.2047596)
11. Spence A, Sharp P. 1985 Self-similar solutions for elastohydrodyamic cavity flow. *Proc. R. Soc. Lond. A* **400**, 289–313. (doi:10.1098/rspa.1985.0081)
12. Desroches J, Detournay E, Lenoach B, Papanastasiou P, Pearson JRA, Thiercelin M, Cheng A. 1994 The crack tip region in hydraulic fracturing. *Proc. R. Soc. Lond. A* **447**, 39–48. (doi:10.1098/rspa.1994.0127)
13. Hubbert MK, Willis DG. 1957 Mechanics of hydraulic fracturing. *Petrol. Trans.* **210**, 239–257.
14. Bunger AP. 2006 A photometry method for measuring the opening of fluid-filled fractures. *Meas. Sci. Technol.* **17**, 3237–3244. (doi:10.1088/0957-0233/17/12/006)
15. Kavanagh JL, Menand T, Sparks RSJ. 2006 An experimental investigation of sill formation and propagation in layered elastic media. *Earth Planet. Sci. Lett.* **245**, 799–813. (doi:10.1016/j.epsl.2006.03.025)
16. Bunger AP, Detournay E. 2008 Experimental validation of the tip asymptotics for a fluid-driven crack. *J. Mech. Phys. Solids* **56**, 3101–3115. (doi:10.1016/j.jmps.2008.08.006)
17. Kavanagh JL, Menand T, Daniels KA. 2013 Gelatine as a crustal analogue: determining elastic properties for modelling magmatic intrusions. *Tectonophysics* **582**, 101–111. (doi:10.1016/j.tecto.2012.09.032)
18. Di Giuseppe E, Funiciello F, Corbi F, Ranalli G, Mojoli G. 2009 Gelatins as rock analogs: a systematic study of their rheological and physical properties. *Tectonophysics* **473**, 391–403. (doi:10.1016/j.tecto.2009.03.012)
19. Long R, Hall MS, Wu M, Hui CY. 2011 Effects of gel thickness on microscopic indentation measurements of gel modulus. *Biophys. J.* **101**, 643–650. (doi:10.1016/j.bpj.2011.06.049)
20. Sneddon IN. 1951 *Fourier transforms*. New York, NY: McGraw-Hill.
21. Spence DA. 1968 Self-similar solutions to adhesive contact problems with incremental loading. *Proc. R. Soc. Lond. A* **305**, 55–80. (doi:10.1098/rspa.1968.0105)